Sugar-based amphiphilic nanoparticles arrest atherosclerosis in vivo

Daniel R. Lewis[a,b,1], Latrisha K. Petersen[b,1], Adam W. York[b], Kyle R. Zablocki[b], Laurie B. Joseph[c], Vladyslav Kholodovych[d], Robert K. Prud'homme[e], Kathryn E. Uhrich[f], and Prabhas V. Moghe[a,b,2]

[a]Department of Chemical & Biochemical Engineering, [b]Department of Biomedical Engineering, [c]Department of Pharmacology, [f]Department of Chemistry and Chemical Biology, and [d]Office of Information Technology, Division of High Performance & Research Computing, Rutgers University, Piscataway, NJ 08854; and [e]Department of Chemical & Biomolecular Engineering, Princeton University, Princeton, NJ 08544

Edited by Robert Langer, Massachusetts Institute of Technology, Cambridge, MA, and approved January 16, 2015 (received for review December 28, 2014)

Atherosclerosis, the build-up of occlusive, lipid-rich plaques in arterial walls, is a focal trigger of chronic coronary, intracranial, and peripheral arterial diseases, which together account for the leading causes of death worldwide. Although the directed treatment of atherosclerotic plaques remains elusive, macrophages are a natural target for new interventions because they are recruited to lipid-rich lesions, actively internalize modified lipids, and convert to foam cells with diseased phenotypes. In this work, we present a nanomedicine platform to counteract plaque development based on two building blocks: first, at the single macrophage level, sugar-based amphiphilic macromolecules (AMs) were designed to competitively block oxidized lipid uptake via scavenger receptors on macrophages; second, for sustained lesion-level intervention, AMs were fabricated into serum-stable core/shell nanoparticles (NPs) to rapidly associate with plaques and inhibit disease progression in vivo. An AM library was designed and fabricated into NP compositions that showed high binding and down-regulation of both MSR1 and CD36 scavenger receptors, yielding minimal accumulation of oxidized lipids. When intravenously administered to a mouse model of cardiovascular disease, these AM NPs showed a pronounced increase in lesion association compared with the control nanoparticles, causing a significant reduction in neointimal hyperplasia, lipid burden, cholesterol clefts, and overall plaque occlusion. Thus, synthetic macromolecules configured as NPs are not only effectively mobilized to lipid-rich lesions but can also be deployed to counteract atheroinflammatory vascular diseases, highlighting the promise of nanomedicines for hyperlipidemic and metabolic syndromes.

atherosclerosis | nanomedicine | biomaterials | macrophages

Cardiovascular disease is responsible for one in every three deaths in the United States (1). Chronically high circulating levels of low-density lipoprotein (LDL) deposit and undergo oxidation (oxLDL) within arterial walls, which consequently stimulates endothelial inflammation and recruitment of circulating monocytes (2). These recruited cells differentiate into macrophages that overexpress scavenger receptors (SR), which internalize oxLDL in an unregulated fashion, propagating the inflammatory cascade and leading to multifocal sites of neo-intimal plaques (3, 4). The prevalent cardiovascular therapeutics, which are focused on lowering circulating levels of LDL, are unable to directly target these developing atherosclerotic lesions (5).

To address this unmet need, nanoassemblies have been designed to reach narrow vessels and abrogate the lipid deposition and atheroinflammatory phenomena that catalyze plaque establishment, growth, and ensuing acute or chronic cardiovascular events (6). Reports on recent advances in amphiphilic micelles require release of pharmacologic factors to counteract plaque aggravation and local delivery or the conjugation of targeting ligands to reach areas of atherosclerotic lesions (7–9). The major unresolved challenge to repressing atherogenesis lies in the design of serum-stable systems, targeted to lesion SRs, which can have a long-term impact on plaque dynamics (10, 11).

Sugar-based amphiphilic macromolecules (AM) have been conceptualized as fully synthetic constructs that exhibit binding to SRs by mimicking the charge and hydrophobicity of oxidized lipoproteins (12). Using both in vitro and in silico models, AMs were found to competitively bind macrophage SRs, thus inhibiting modified lipid internalization and foam cell formation (13–15). When complexed around hydrophobic core solutes using kinetic fabrication techniques, the AMs form nanoparticles (NPs) that display resistance to unimer release in serum-rich environments (16, 17). Presentation of AMs as NPs established a unique modular design, which could be tuned to alter SR expression in vitro, switching macrophages to an antiatherogenic phenotype (18). Despite these advances, in the absence of a rational materials design strategy, AM therapeutics that elicit superior biodistribution, lesion retention, and lipid burden management in vivo have yet to be realized.

In this study, we propose a new paradigm of atherosclerotic therapeutics founded on the rational design, screening, and identification of highly atheroprotective, sugar-based AM compositions integrated within serum-stable NPs (Fig. 1). The central hypothesis is that by targeting atherogenic macrophages, AM NPs will show preferential accumulation at the sites of atherosclerotic plaques and arrest the critical conversion of macrophages to foam cells and the ensuing atheroinflammation. To evaluate this hypothesis, serum-stable, modular NPs were kinetically fabricated with structurally diverse AMs that varied in hydrophobicity, rigidity, charge, and stereochemistry. In contrast to the traditional unitary endpoints of efficacy, a multivariate "atheroprotective" biological feature space was envisioned to

Significance

Lipid-rich plaques in major blood vessels recruit macrophages that further exacerbate the lipid burden and risk of heart attacks or stroke. A local approach to prevent plaque growth has yet to be successfully deployed. In this study, we examine how synthetic ligands counteract macrophage atherogenesis and de-escalate plaque burden. Using a library of sugar-based amphiphilic core-shell layered nanoparticles, we demonstrate the design principles necessary to prevent oxidized lipid uptake and suppress scavenger receptor expression in macrophages, switching them to an "atheroprotective" phenotype. When administered in vivo, nanoparticles were retained at atherosclerotic lesions, where they mitigated cholesterol clefts, inflammation, and artery occlusion. Thus, synthetic nanomedicines could be used to potentially treat acute coronary syndrome, a major unmet need in cardiovascular diseases.

Author contributions: D.R.L., L.K.P., A.W.Y., K.R.Z., L.B.J., K.E.U., and P.V.M. designed research; D.R.L., L.K.P., A.W.Y., K.R.Z., and V.K. performed research; L.B.J., V.K., R.K.P., and K.E.U. contributed new reagents/analytic tools; D.R.L., L.K.P., V.K., and P.V.M. analyzed data; and D.R.L., L.K.P., R.K.P., K.E.U., and P.V.M. wrote the paper.

The authors declare no conflict of interest.

This article is a PNAS Direct Submission.

[1]D.R.L. and L.K.P. contributed equally to this work.

[2]To whom correspondence should be addressed. Email: moghe@rutgers.edu.

This article contains supporting information online at www.pnas.org/lookup/suppl/doi:10.1073/pnas.1424594112/-/DCSupplemental.

guide the rational screening of NPs. Three coupled phenomena that converge to enhance lesion targeting and inhibit macrophage foam cell conversion were considered for the materials design: (*i*) graded binding to the primary scavenger receptors [macrophage scavenger receptor 1 (MSR1), CD36] to aid lesion accumulation; (*ii*) competitive inhibition of oxLDL uptake; and (*iii*) down-regulation of the cell surface expression of MSR1 and CD36. The most atheroprotective NP composition was identified through this multidimensional screening platform, validated via structure–activity correlations and administered to challenge atherosclerotic development in vivo. We report lesion localization and therapeutic efficacy in atherosclerotic ApoE$^{-/-}$ mice, indicating the potential for synthetic AM NPs as therapeutic agents for plaque management in coronary artery disease.

Results

AM NPs with Comprehensive Atheroprotective Profiles Can Be Identified. SR-mediated unregulated uptake of oxidized lipids, the ensuing inflammatory signaling in plaque macrophages, and subsequent narrowing of the artery are key features of atherosclerosis that motivated the design of AM NPs. oxLDL, which binds SRs on plaque-resident macrophages, plays a key role in the progression of atherosclerosis; thus, the NPs were designed to mimic select physiochemical and structural features of oxLDL as a strategy to counteract oxLDL-SR binding. To design a therapeutic with these characteristics, screening and evaluation methodologies were developed. AMs with varying charge, hydrophobicity, and stereochemistry (Fig. 2*A*) were synthesized, guided by the hypothesis that these are critical features for SR binding (19). These AMs were then used as graded "shells" to engineer a library of AM NPs using flash nanoprecipitation around a common hydrophobic core solute (Fig. 2*B*). The mucic acid-based hydrophobe M_{12} was used as the core molecule because of the matched hydrophobicity with the AMs, resulting in stable, monodisperse NPs (*SI Appendix*, Fig. S1). The library of NP formulations was then evaluated in vitro using human monocyte-derived macrophages (hMDMs) for atherogenic endpoints, including accumulation of modified lipids (Fig. 2*C*), SR-mediated uptake (Fig. 2*D*), and modulation of SR expression (Fig. 2*E*).

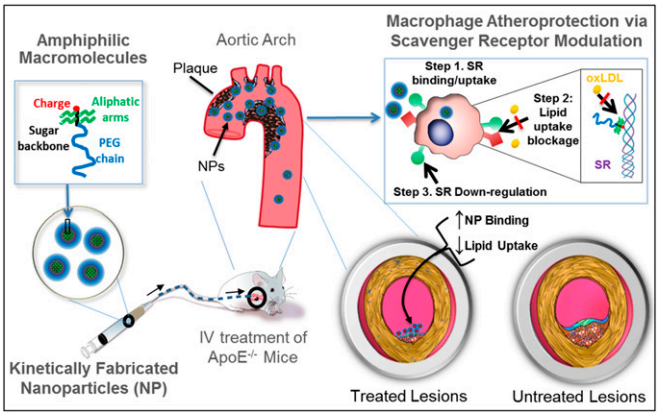

Fig. 1. The envisioned paradigm to counteract atherosclerotic plaque development aims to repress lipid-scavenging receptors at the level of lesion-based macrophages. Sugar-based AMs were designed to competitively block oxLDL uptake via binding and regulation of SRs on human macrophages. A library of AMs, with systematic variations in charge, stereochemistry, and sugar backbones, was synthesized and kinetically fabricated into serum-stable, core/shell NPs and screened in vitro to identify shell architectures that exhibited maximal atheroprotective potency. To demonstrate lesion-level intervention, the lead NP was administered in an atherosclerosis animal model to challenge lesion development during coronary artery disease.

Interestingly, the NPs with shell AMs composed of specific stereochemistry with chiral symmetry, M_{12}PEG, bM_{12}PEG, cM_{12}PEG, aM_{12}PEG, and $T^{Meso}{}_{12}$PEG, prevented the uptake of oxLDL in cultured hMDMs to a greater extent than AMs with alternate stereochemistries (Fig. 2*C*). Many of these same stereochemistries also demonstrated significant binding and cellular uptake via SR MSR1; notably, within this group only M_{12}PEG and aM_{12}PEG revealed binding to CD36 (Fig. 2*D* and *SI Appendix*, Fig. S2*A*). These data suggest a relationship between MSR1 binding and oxLDL inhibition, and that specific stereochemistries best enhance these effects. We hypothesize that the NPs bind to SRs in competition with oxLDL, and that by occupying the receptors critical for oxLDL uptake, the NPs inhibit the cellular accumulation of modified lipids. Specific stereochemistries may allow for better orientation of the AM shell hydrophobic arms and charge apposition with the SR binding domains for oxLDL, enabling more efficient blockage of hydrophobic binding domains of SRs (20). Finally, to evaluate the atheroprotective effects of NPs, we screened the ability of NP formulations to down-regulate scavenger receptor surface expression. Several of the most potent oxLDL-inhibiting and MSR1-binding NP formulations also revealed the ability to down-regulate MSR1 and CD36 surface expression, specifically the NPs with M_{12}PEG, bM_{12}PEG, cM_{12}PEG, and $T^{Meso}{}_{12}$PEG as shell compositions (Fig. 2*E* and *SI Appendix*, Fig. S2*B*). Similar down-regulation of gene expression was also observed for both SRs (*SI Appendix*, Fig. S3). These results suggests that, in addition to receptor binding, the NPs are able to disrupt the cycle of SR replenishment induced by oxLDL that leads to uncontrolled oxLDL uptake and foam cell formation. In contrast, control polystyrene-based NP system (composed of nonbioactive PS_{14}PEG shell and PS_{14} core) exhibited no biological activity (*SI Appendix*, Fig. S4).

By reviewing the cumulative screening endpoints, correlations emerged between SR binding/uptake, SR expression modulation, and degree of oxLDL inhibition, demonstrating that multivariate outcomes can now be used as the foundational elements for designing potential antiatherosclerotic therapeutics (Fig. 2*F*). The matrix shows the correlations for all AM NP compositions. When the cumulative outcomes of the five biological endpoints of different NPs were aggregated, the strongest atheroprotective profile was identified for M_{12}PEG, which was selected as the lead composition for translational studies (Fig. 2*G*). A parallel modeling effort was also conducted to establish a structure–activity relationship framework for predictive in silico screening and further evolution of AM candidates. Using quantitative structure–activity relationship models for each of the in vitro endpoints tested, based on previously identified 3D structures of AMs (13), molecular descriptors that highly correlated with biological activity were found (*SI Appendix*, Fig. S5).

Next, we confirmed that NPs based on M_{12}PEG shell composition were not only effective at reducing the foam cell phenotype (*SI Appendix*, Fig. S6) but were also highly stable, capable of maintaining antiatherosclerotic efficacy for at least 300 d (*SI Appendix*, Fig. S7).

Atheroprotective NPs Exhibit Slow Circulation Clearance and Broad Biodistribution. NPs offer the capability to overcome two primary challenges in drug design: bioavailability and the ability to specifically localize to the disease site. Following administration of the lead NP formulation, M_{12}PEG, to ApoE$^{-/-}$ mice with advanced atherosclerotic lesions (Fig. 3*A*), these endpoints were evaluated by examining NP serum concentration, whole-body distribution, and specific tissue localization. Mice were repeatedly injected on a weekly basis to ensure that therapeutic levels of AM NPs above 10^{-7} M were present in arteries over a time frame that would impact lesion development. Postinjection, the NPs exhibited homogenous distribution throughout the body that correlated to serum NP concentrations (Fig. 3*A*). The NPs displayed relatively long in vivo half-lives of ~28 h, considerably longer than conventional micellar systems designed to target and treat atherosclerosis (8). The M_{12}PEG NPs evaluated in this work have an

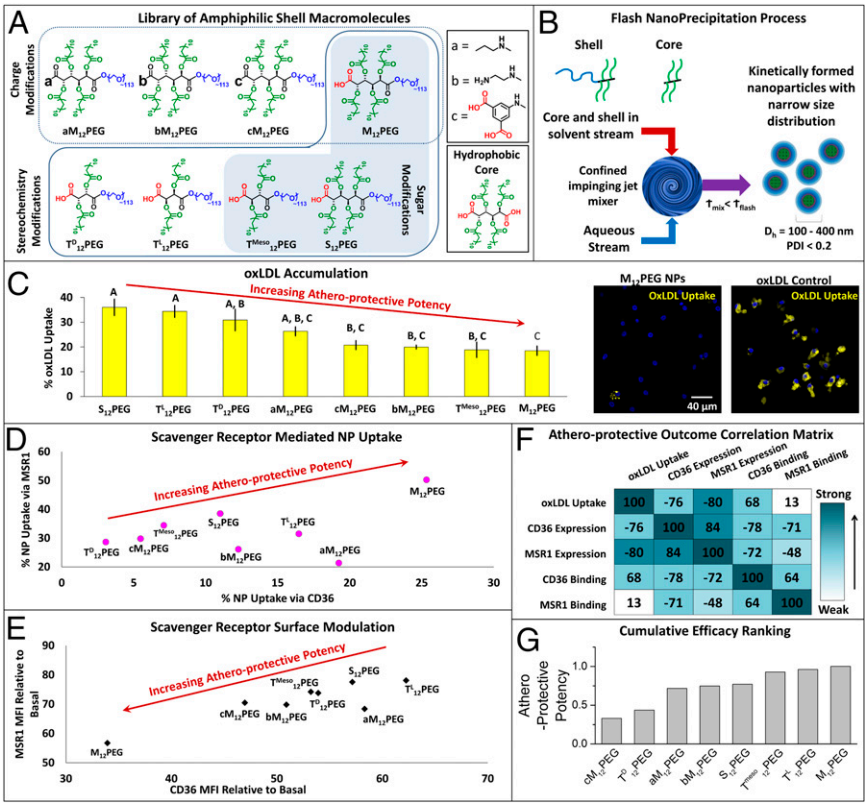

Fig. 2. AM NPs were designed, fabricated, and screened for multiple measures of bioactivity, and the most atheroprotective NP formulation was identified. (*A*) A library of AMs, with changes in charge, stereochemistry, and sugar backbones, was designed and synthesized, and (*B*) kinetically fabricated into serum-stable, core/shell nanoparticles via flash nanoprecipitation. In vitro screening of NP bioactivity was measured via several atherogenic endpoints in hMDMs: (*C*) inhibition of oxLDL accumulation, (*D*) NP binding and uptake via key scavenger receptors MSR1 and CD36, and (*E*) NP modulation of surface expression of MSR1 and CD36. (*F*) Correlation analysis found varied relationships between these five measures of atheroprotective outcomes. (*G*) The biological outcomes were weighted and NPs were cumulatively ranked for efficacy. For *C* and *E*, the cells were coincubated with 5 μg/mL oxLDL and 10^{-5} M NPs for 24 h, whereas for *D*, the cells were incubated with polyinosinic acid (MSR1 inhibitor) or CD36 blocking antibody (CD36 inhibitor) for 2 h and then incubated with 10^{-5} M NPs for 6 h, and all analysis was evaluated by flow cytometry. Error bars represent SEM and $n = 3$. For *C*, all treatments are $P < 0.0001$ from oxLDL only control and those with the same letter are statistically indistinguishable. The control nonbioactive nanoparticle (PS_{14}PEG shell, PS_{14} core) demonstrated no atheroprotective bioactivity (*SI Appendix*, Fig. S4).

average size of 160 nm, with narrow size distribution (*SI Appendix*, Fig. S1). In addition to long bioavailability, the NPs showed promising organ distribution, with low levels of accumulation in all organs at the terminal time point. Most NPs not bound to lesions were retained in the liver, indicating hepatic clearance and metabolism of circulating NPs (Fig. 3*B*). Furthermore, the lack of fluorescence in the lungs demonstrates that the small and flexible M_{12}PEG NPs do not agglomerate and become trapped in capillary beds. Minimal accumulation of the M_{12}PEG NPs in the spleen indicates that they will not interfere with filtration of red blood cells or activation of lymphocytes (21). Following degradation of the NPs into their core and shell components, they are likely cleared via renal filtration because of the small unimer size and via hepatic metabolism, which is supported by ex vivo fluorescence of the kidneys and liver. Interestingly, the control NP formulation (PS_{14}PEG shell and PS_{14} core) revealed high levels of fluorescence in the liver, spleen, and kidneys, suggesting significant accumulation with minimal metabolism (*SI Appendix*, Fig. S8).

NPs Localize to Atherosclerotic Plaques. To validate the atherosclerotic lesion-specific delivery and localized therapeutic potential of the NPs, the aortas of $ApoE^{-/-}$ mice were examined at both macroscopic and microscopic levels for the presence of NPs. After 16 wk of a Western diet, nontreated (NT) $ApoE^{-/-}$ mice had stage IV lesions along the ascending aorta and arch that macroscopically appear as white ingrowths in the intima of the aorta. En face ex vivo fluorescence imaging of the aortic tree revealed specific lesion targeting of NPs to atherosclerotic plaques of varying severity (Fig. 4*A*). NP fluorescence (Fig. 4*A*, red) can be seen overlapping with the opaque plaque dominant regions of the aorta (Fig. 4*A*, white), especially at the far right region containing the aortic arch. The aortic arch and carotid branch points are areas of largest plaque burden in $ApoE^{-/-}$ mice because of the combination of high pressure and low shear stress that accompanies turbulent blood flow (22, 23). Quantitative fluorescence imaging of the aorta (Fig. 4*B*) revealed that these areas exhibited the highest concentration of NPs throughout the aortic tree (Fig. 4*C*). NPs localized around the necrotic core within plaques, as seen by confocal microscopy (Fig. 4*D*). This targeting effect is most likely a result of the negatively charged NPs with optimal stereochemistry and rigidity, displaying affinity to the positively charged SR binding domains on atherogenic macrophages and activated endothelia (15). SRs are commonly overexpressed on plaques, providing target receptors for NP localization (10). The high levels of NP binding to areas of plaque appear to be directly correlated with in vitro binding to SR and uptake by macrophages. This result is noteworthy as the NP-based presentation of low-affinity macromolecules to SRs is sufficient for plaque localization. When individual cell types within aortas were probed, the NPs were found preferentially associated with cells expressing vascular cell-adhesion molecule (VCAM) (Fig. 4*E*).

NPs Lower Artery Occlusion by Reducing Lipid Accumulation, Neointimal Hyperplasia, and Inflammatory Signaling. The ability of NPs to stop disease progression was demonstrated by examining the plaque size and morphology in $ApoE^{-/-}$ mice. Cross-sections of the aortas in untreated mice were characterized by the presence of large fibrous plaques with necrotic cores and cholesterol clefts characteristic of advanced disease (Fig. 5*A*). In contrast, mice treated with NPs had morphologically less-developed lesions and showed a significant reduction (37%) in artery occlusion compared with the nontreated mice (Fig. 5*C*). AM NPs were able to stabilize arteries by mitigating the coupled endpoints of lipid accumulation (Oil Red O), inflammation (COX-2), and neointimal hyperplasia [smooth muscle cell (SMC) α-actin], demonstrating efficacy in this model of human atherosclerotic disease (Fig. 5*B*). We hypothesize that, following penetration into the atherosclerotic plaques, the NPs bind scavenger receptors of plaque-resident cells and prevent oxidized lipid-cellular interactions. By decreasing lipid accumulation within the artery, local inflammation would be lower and result in an overall reduction in artery occlusion. In contrast to AM NP-treated mice, the histology of lesions in animals treated with control PS_{14}PEG NPs did not show reduced lipid and inflammatory burden (*SI Appendix*, Fig. S9).

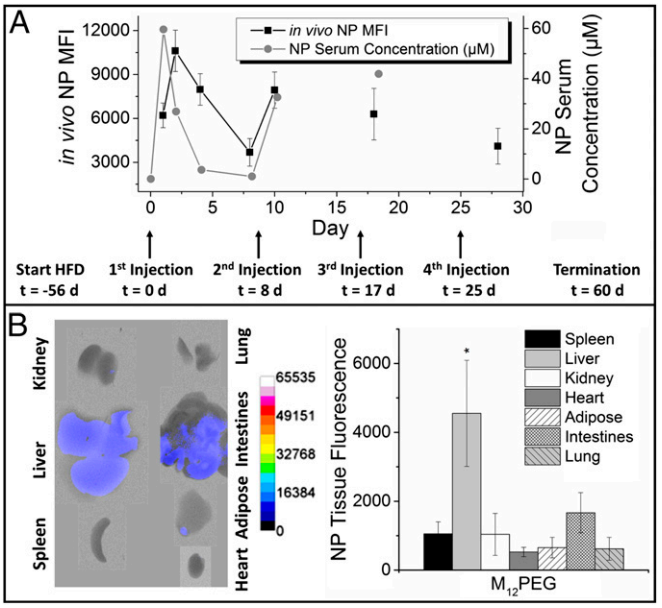

Fig. 3. AM NPs demonstrated sustained blood circulation and minimal organ accumulation. (*A*) M_{12}PEG was administered in vivo to ApoE$^{-/-}$ mice over a four-dose regimen for evaluation of whole body and organ biodistribution and serum pharmacokinetics. NPs had rapid, homogenous distribution and long serum half-lives after injection time points (arrows). Ex vivo fluorescence images (*B*, *Left*) and quantification (*Right*) show minimal organ accumulation with M_{12}PEG, with some residual NPs in the liver. Error bars represent SEM and $n = 5$. *$P < 0.05$ from the control (NT). Biodistribution and pharmacokinetics for control PS_{14}PEG NP treatment can be found in *SI Appendix*, Fig. S8.

Discussion

Atherosclerosis presents one of the most challenging etiologies for vascular occlusive diseases, causing widespread lipid burden within the intima of major arteries, and triggering a wide range of adverse outcomes. Conventional approaches to manage atherosclerotic disease have either focused on maintaining the patency of lesioned blood vessels via ballooning and implantation of interventional stent devices (24), or systemically administering drugs that lower circulating cholesterol synthesis (25). Neither approach fundamentally alters the dynamics within existing plaques because atherosclerotic progression is primarily tied to the pivotal sequence of: (*i*) reduced LDL trafficking, (*ii*) intimal retention and oxidation, and (*iii*) foam cell conversion in macrophages. In this report, we present amphiphilic macromolecule nanoparticles (AM NPs) that have high levels of retention at atherosclerotic plaques and show progressive disease stabilization, thus exhibiting the critical design prerequisites for new lesion-directed atherosclerotic therapeutics.

The modular composition of AMs allows for a wide library of features with modifications in the charge, hydrophobicity, and stereochemistry (13, 26). A key aspect of this work is the design of composite nanoparticles with different shell AMs, thus generating a graded library of therapeutics. The M_{12} core shared among the different NPs was chosen to match the hydrophobic domain of the AMs, imparting strong resistance to the core release and stability in serum-rich environments. The most potent NP configurations identified in this work appear to be enabled by shell AMs with specific stereochemistry, which elicited enhanced binding to the hydrophobic binding domains of SRs, thought to be key for inhibiting the internalization of oxLDL (20). By competing for SR, the NPs effectively reduce oxLDL uptake and the ensuing foam cell phenotype in hMDMs, indicating that the NPs displaying these AMs are binding with higher avidity and preventing oxLDL trafficking into macrophages. This finding is consistent with previous in silico molecular dynamics models of AMs, which indicate that the 3D structure is the strongest determinant of efficacy at inhibiting oxLDL uptake, specifically the extended conformation of the hydrophobic arms (13).

The NPs used in this study exhibit two complementary features: first, AMs that bind SRs and inhibit oxidized lipid uptake, the effects of which are amplified by multimeric presentation via nanoparticles; and second, the ability to down-regulate SR expression, causing a longer term antiatherogenic phenotype. Taken together, these attributes enable the multivariate comparative screening of a library of different NPs using a ranking of "atheroprotective potency"; this determined that antiatherogenic endpoints were highly correlated for some NPs and identified a lead candidate for in vivo testing. The datasets from this study also serve as the building blocks for a computational model, necessary for a novel class of drugs with a unique mechanism of action (27), and for predicting novel AM structures in the future.

The ability of the NPs to maintain biological efficacy in the presence of serum and to partition into sites of atherosclerotic lesions within the aortic arch are two critical properties to the sustained bioavailability of NPs at the lesion sites. A key advantage of the AM NPs lies in their ability to preferentially deposit into lesions without specific peptide or antibody conjugation. Targeting ligands can be immunogenic and may not be able to confer the broad-spectrum specificity to varying stages of plaque development seen with AM NPs (28). In contrast, the

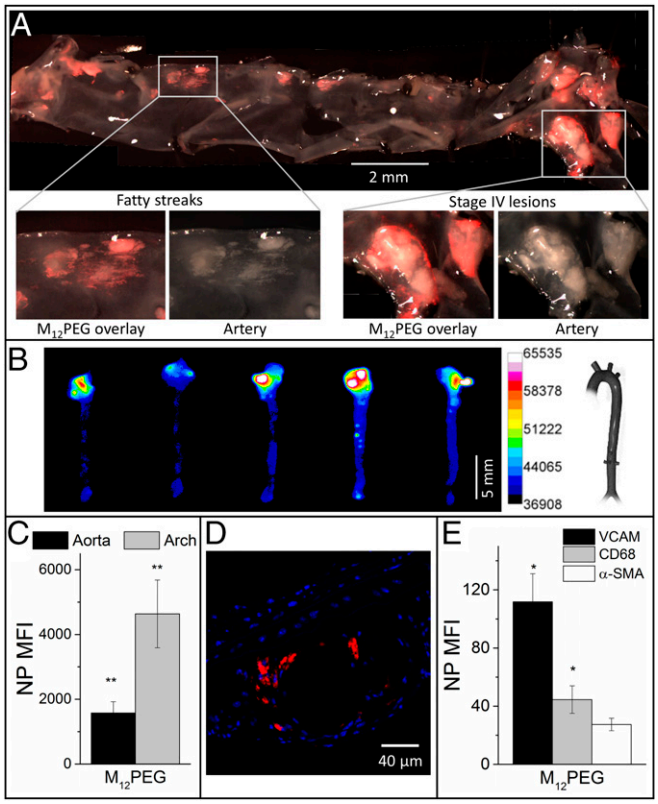

Fig. 4. AM NPs demonstrated significant localization at developing atherosclerotic lesions. (*A*) En face aorta fluorescence images revealed specific lesion targeting by M_{12}PEG (red) at 24 h postinjection. (*B* and *C*) Ex vivo fluorescence images show the highest levels of NP accumulation remained in the aortic arch at 60 d postinitial injection. (*D*) Confocal microscopy confirmed NP accumulation (red) within atherosclerotic plaques, localized around a necrotic lipid core. (*E*) NPs were primarily associated with cells expressing VCAM1 and CD68, as determined by flow cytometry. Error bars represent SEM and $n = 5$. *$P < 0.05$ from the control (NT); **$P < 0.001$ from the control (NT). Lesion localization of control PS_{14}PEG NPs can be found in *SI Appendix*, Fig. S9 *A* and *B*.

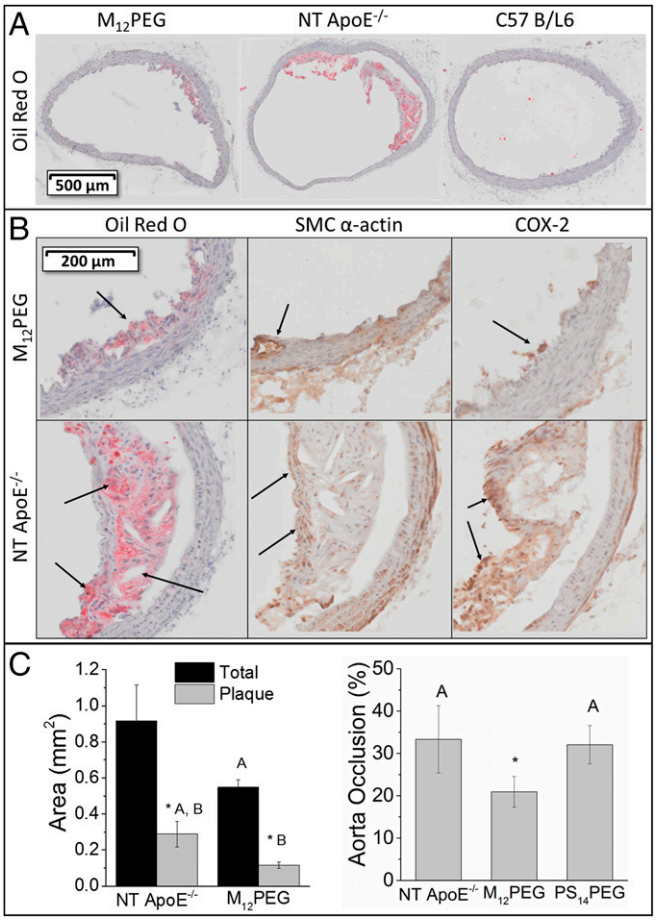

Fig. 5. AM NPs demonstrated in vivo efficacy at mitigating atherosclerotic endpoints upon intravenous administration in ApoE$^{-/-}$ mice. (*A*) Aortic cross sections stained with Oil Red O showed a dramatic reduction in lipid burden and plaque development. (*B*) Regions of plaque formation within mouse aortic tissues highlighting M_{12}PEG efficacy at lowering lesion severity, including the prevention of lipid buildup and cholesterol cleft formation (arrows in Oil Red O images), neointimal hyperplasia (arrows in SMC α-actin images), and inflammation (arrows in COX-2 images). (*C*) Treatment with M_{12}PEG resulted in a 37% decrease in aorta occlusion, but PS_{14}PEG NPs were not effective at reducing occlusion. Vessel occlusion was determined by quantifying plaque as a fraction of vessel area for serial aortic cross sections. Error bars represent SEM and $n = 5$. *$P < 0.05$ from the control (NT), treatments with the same letter are statistically indistinguishable. Histology for control PS_{14}PEG NPs treatment can be found in *SI Appendix*, Fig. S9 *B* and *C*.

nanoscale presentation of AMs via the NPs elevates the net binding affinity of the AMs for SRs, leading to enhanced lesion retention and association with macrophages and activated endothelia (14). AM NP targeting may also occur because of the damaged endothelial lining covering plaques, enabling enhanced permeability and retention of nanoscale particles (6, 29). Within advanced plaques, the NPs localized to the periphery, surrounding the necrotic core, where most atherogenic macrophages reside. This area is extremely vulnerable to degradation by secreted proteases, which can thin the fibrous cap, leading to plaque rupture. By targeting these cells specifically, it may be possible to stabilize vulnerable plaques (30). The biodistribution and pharmacokinetic profile of NPs also highlights the benefits of kinetically fabricated particles relative to micelles, validating previous in vitro stability studies in the presence of serum (8, 16). The larger size of intact NPs relative to micelles may also protect them from renal filtration, which has a size cut-off of ~8 nm, thus enabling longer circulation times (31). Other mechanisms, such as PEG shielding to resist protein binding and agglomeration, can also maintain NP hydrodynamic diameters smaller than lung capillary mechanical filtration size of 4–10 μm (32).

The AM NPs were observed to mitigate several coupled endpoints of atherosclerotic phenomena, namely lipid accumulation, SMC proliferation, inflammation, and artery occlusion in the ApoE$^{-/-}$ mouse model. Treatment with NPs markedly improved the morphology of lesions in treated animals, minimizing cholesterol clefts and the presence of necrotic lipid cores. Histology indicates that NP binding to plaques was a consequence of the composition of the AMs and likely correlates primarily with the presence of atherogenic macrophages, and secondarily to activated endothelial cells and SMCs expressing high levels of SR and adhesion molecules. Preliminary data in our laboratories also suggest that AMs protect endothelia from oxLDL uptake, potentially via SRs, as well as through decreased monocyte adhesion. Similarly, the NPs could block scavenger receptor-mediated oxLDL-effects on smooth muscle cell activation and proliferation, which can contribute to occlusion of blood flow, thus potentially providing a more sustained repression of the early atheroinflammatory cascade in lesions (33). Despite the success of the AM NPs reported here, one of the plausible limitations of the current mechanism of action is that it is geared toward preventing the development of early atherosclerotic disease. Future improvements in the design could involve combination approaches that rescue advanced lesions by promoting reverse cholesterol transport, potentially by drug encapsulation (7).

In conclusion, we demonstrate the promise of novel nanomedicines that exhibit site-directed treatment of atherosclerosis. Several new areas of application can be envisioned, specifically the treatment of blood vessels that cannot be stented, such as long peripheral arteries and surrounding microvasculature that develop multifocal and diffuse lipid burden-related disease, leading to claudication, limb ischemia, and amputations. A particularly promising implication from the observed mechanism-of-action of AM NPs is that they could potentially repress the development of vulnerable plaques, which are characterized by a lipid rich necrotic core, a thin fibrous cap, and high macrophage burden (30). Thus, the AM NPs could potentially reduce the risk of rupture and clot formation, which remains a major unmet challenge for acute coronary syndromes in cardiovascular disease.

Materials and Methods

Materials and methods are briefly described here. Further details are in the *SI Appendix*.

NP Fabrication and Characterization. AMs were synthesized as previously described (19, 26, 34, 35) and fabricated into kinetically assembled fluorescent NPs via flash nanoprecipitation (16, 17). NP shell structures are depicted in Fig. 1 and the cores were composed of mucic acid acylated with lauryl groups (M_{12}). NPs were fluorescently labeled with AlexaFluor680 or ETtP5 for tracking. Control NPs were fabricated from polystyrene-block-poly(ethylene glycol) shells and polystyrene cores (PS_{14}PEG). NP size and polydispersity index were determined by dynamic light scattering using a Zetasizer Nano ZS (Malvern).

In Vitro Evaluation of AM NP Efficacy. NPs were evaluated for efficacy by measurement of oxLDL uptake inhibition, ability to bind scavenger receptors MSR1 and CD36, and ability to modulate scavenger receptor expression in hMDMs (13, 18).

Correlation Analysis and Computational Model. Efficacy data for oxLDL uptake inhibition, NP uptake by MSR1, NP uptake by CD36, down-regulation of MSR1 surface expression, and down-regulation of CD36 surface expression were converted into a database in molecular operating environment v2013.08 (Chemical Computing Group). A correlation matrix was calculated for all measured biological endpoints in molecular operating environment. For ranking of cumulative atheroprotective potency, all in vitro efficacy values were normalized, weighted equally, and summed for each NP formulation. NPs were rank ordered and the highest-performing NP (M_{12}PEG) was selected for further studies. Additionally, a predictive computational model was also established to compare the molecular structure–activity relations based on the in vitro endpoint efficacy values.

Animals. Four-week-old B6.129P2-*Apoe*^{tm1Unc} (ApoE$^{-/-}$) and C57B/L6 mice were given free access to food and water. ApoE$^{-/-}$ mice were fed Harlan Teklad diet TD.88137 and C57B/L6 mice were given standard chow diet. The Rutgers University Institutional Committees on Animal Care and Use approved all procedures involving animals (protocol 06-016).

AM NP Administration. NPs were injected via the tail vein at day 0, 8, 17, and 25 to ApoE$^{-/-}$ mice after 8 wk on the Western diet.

Animal Imaging. To determine biodistribution over time, mice were imaged live with a MultiSpectral FX Pro In Vivo Imager (Carestream) before NP administration and at 1, 2, 4, 8, 10, 18, and 26 d after the initial NP administration.

NP Pharmacokinetics. Blood samples were withdrawn through the saphenous vein and serum was measured for AF680 fluorescence on a Tecan M200 Pro and normalized using a standard curve. For pharmacokinetic parameter determination, the half-life was calculated assuming a one-compartment model.

NP Cellular Association and Receptor Expression Using Flow Cytometry. Single-cell suspensions were prepared from the abdominal aorta, incubated with the appropriate antibody for CD68, VCAM1, and SMC α-actin (Biolegend) and then quantified (10,000 cellular events per sample) using a Gallios flow cytometer (Beckman Coulter).

Aorta Tissue Preparation for Imaging and Immunohistochemistry. The ascending aorta and aortic arch were sectioned serially to examine plaque morphology and binding of AM NPs to lesions. Sections were stained with Oil Red O, SMC α-actin, and COX-2 for inflammation and imaged using an Olympus VS-120 or Leica TCS SP2.

Image Analysis. Fluorescence images (mouse whole-body and ex vivo organs) were quantified using ImageJ. The background from nontreated groups was subtracted from total fluorescence intensity, which was then normalized to area. Aortic cross sections were quantified for total and plaque area using VS-AFW software (Olympus).

Statistical Analysis. Results are presented as mean ± SEM and were evaluated by one-way ANOVA with post hoc Tukey's test for comparisons between multiple conditions or Student's *t* test for individual comparisons. A *P* value of 0.05 or less was considered statistically significant.

ACKNOWLEDGMENTS. We thank Allison Faig, Li Gu, Dawanne Poree, Dalia Abdelhamid, Yingyue Zhang, Ricky Li, Rebecca Chmielowski, Sonali Ahuja, and John Chae for technical help, and Prof. John Anthony from the University of Kentucky, Department of Chemistry for the ETtP5. This study was supported in part by National Heart, Lung and Blood Institute Grants R01HL107913 and R21HL93753 (to P.V.M. and K.E.U.); the Coulter Foundation for Biomedical Engineering Translational Research Award (to P.V.M.); National Institutes of Health T32 training programs and Fellowships EB005583 (to A.W.Y.) and T32GM008339 (to D.R.L.); and the National Institutes of Health CounterACT Program through the National Institute of Arthritis and Musculoskeletal and Skin Diseases Grant U54AR055073 (to L.B.J.).

1. Roger VL, et al.; American Heart Association Statistics Committee and Stroke Statistics Subcommittee (2012) Heart disease and stroke statistics—2012 update: A report from the American Heart Association. *Circulation* 125(1):e2–e220, and erratum (2012) 125(22):e1002.
2. Libby P, Ridker PM, Maseri A (2002) Inflammation and atherosclerosis. *Circulation* 105(9):1135–1143.
3. Sahoo D, Drover V (2006) The role of scavenger receptors in signaling, inflammation and atherosclerosis. *Biochemistry of Atherosclerosis*, ed Cheema S (Springer, New York), pp 70–91.
4. Fuhrman B, Partoush A, Volkova N, Aviram M (2008) Ox-LDL induces monocyte-to-macrophage differentiation in vivo: Possible role for the macrophage colony stimulating factor receptor (M-CSF-R). *Atherosclerosis* 196(2):598–607.
5. Bucher HC, Griffith LE, Guyatt GH (1999) Systematic review on the risk and benefit of different cholesterol-lowering interventions. *Arterioscler Thromb Vasc Biol* 19(2): 187–195.
6. Lewis DR, Kamisoglu K, York AW, Moghe PV (2011) Polymer-based therapeutics: Nanoassemblies and nanoparticles for management of atherosclerosis. *Wiley Interdiscip Rev Nanomed Nanobiotechnol* 3(4):400–420.
7. Iverson NM, et al. (2011) Dual use of amphiphilic macromolecules as cholesterol efflux triggers and inhibitors of macrophage athero-inflammation. *Biomaterials* 32(32):8319–8327.
8. Peters D, et al. (2009) Targeting atherosclerosis by using modular, multifunctional micelles. *Proc Natl Acad Sci USA* 106(24):9815–9819.
9. Mulder WJM, et al. (2007) Molecular imaging of macrophages in atherosclerotic plaques using bimodal PEG-micelles. *Magn Reson Med* 58(6):1164–1170.
10. Matsumoto A, et al. (1990) Human macrophage scavenger receptors: Primary structure, expression, and localization in atherosclerotic lesions. *Proc Natl Acad Sci USA* 87(23):9133–9137.
11. Alexis F, Pridgen E, Molnar LK, Farokhzad OC (2008) Factors affecting the clearance and biodistribution of polymeric nanoparticles. *Mol Pharm* 5(4):505–515.
12. Chnari E, Nikitczuk JS, Wang J, Uhrich KE, Moghe PV (2006) Engineered polymeric nanoparticles for receptor-targeted blockage of oxidized low density lipoprotein uptake and atherogenesis in macrophages. *Biomacromolecules* 7(6):1796–1805.
13. Lewis DR, et al. (2013) In silico design of anti-atherogenic biomaterials. *Biomaterials* 34(32):7950–7959.
14. Plourde NM, Kortagere S, Welsh W, Moghe PV (2009) Structure-activity relations of nanolipoblockers with the atherogenic domain of human macrophage scavenger receptor A. *Biomacromolecules* 10(6):1381–1391.
15. Tomasini MD, Zablocki K, Petersen LK, Moghe PV, Tomassone MS (2013) Coarse grained molecular dynamics of engineered macromolecules for the inhibition of oxidized low-density lipoprotein uptake by macrophage scavenger receptors. *Biomacromolecules* 14(8):2499–2509.
16. York AW, et al. (2012) Kinetically assembled nanoparticles of bioactive macromolecules exhibit enhanced stability and cell-targeted biological efficacy. *Adv Mater* 24(6):733–739.
17. Johnson BK, Prud'homme RK (2003) Flash nanoprecipitation of organic actives and block copolymers using a confined impinging jets mixer. *Aust J Chem* 56(10):1021–1024.
18. Petersen LK, et al. (2014) Amphiphilic nanoparticles repress macrophage atherogenesis: Novel core/shell designs for scavenger receptor targeting and down-regulation. *Mol Pharm* 11(8):2815–2824.
19. Hehir S, et al. (2012) Carbohydrate composition of amphiphilic macromolecules influences physicochemical properties and binding to atherogenic scavenger receptor A. *Acta Biomater* 8(11):3956–3962.
20. Puente Navazo MD, Daviet L, Ninio E, McGregor JL (1996) Identification on human CD36 of a domain (155-183) implicated in binding oxidized low-density lipoproteins (Ox-LDL). *Arterioscler Thromb Vasc Biol* 16(8):1033–1039.
21. Swirski FK, et al. (2009) Identification of splenic reservoir monocytes and their deployment to inflammatory sites. *Science* 325(5940):612–616.
22. Fazio S, Linton MF (2001) Mouse models of hyperlipidemia and atherosclerosis. *Front Biosci* 6:D515–D525.
23. Knowles JW, Maeda N (2000) Genetic modifiers of atherosclerosis in mice. *Arterioscler Thromb Vasc Biol* 20(11):2336–2345.
24. Serruys PW, Kutryk MJB, Ong ATL (2006) Coronary-artery stents. *N Engl J Med* 354(5): 483–495.
25. Baigent C, et al.; Cholesterol Treatment Trialists' (CTT) Collaborators (2005) Efficacy and safety of cholesterol-lowering treatment: Prospective meta-analysis of data from 90,056 participants in 14 randomised trials of statins. *Lancet* 366(9493):1267–1278.
26. Iverson NM, Sparks SM, Demirdirek B, Uhrich KE, Moghe PV (2010) Controllable inhibition of cellular uptake of oxidized low-density lipoprotein: Structure-function relationships for nanoscale amphiphilic polymers. *Acta Biomater* 6(8):3081–3091.
27. Jorgensen WL (2004) The many roles of computation in drug discovery. *Science* 303(5665):1813–1818.
28. Marcucci F, Lefoulon F (2004) Active targeting with particulate drug carriers in tumor therapy: Fundamentals and recent progress. *Drug Discov Today* 9(5):219–228.
29. Doyle B, Caplice N (2007) Plaque neovascularization and antiangiogenic therapy for atherosclerosis. *J Am Coll Cardiol* 49(21):2073–2080.
30. Boyle JJ (2005) Macrophage activation in atherosclerosis: Pathogenesis and pharmacology of plaque rupture. *Curr Vasc Pharmacol* 3(1):63–68.
31. Choi HS, et al. (2007) Renal clearance of quantum dots. *Nat Biotechnol* 25(10): 1165–1170.
32. Kreuter J (1996) Nanoparticles and microparticles for drug and vaccine delivery. *J Anat* 189(Pt 3):503–505.
33. Auge N, et al. (2002) Oxidized LDL-induced smooth muscle cell proliferation involves the EGF receptor/PI-3 kinase/Akt and the sphingolipid signaling pathways. *Arterioscler Thromb Vasc Biol* 22(12):1990–1995.
34. Tian L, Yam L, Zhou N, Tat H, Uhrich KE (2004) Amphiphilic scorpion-like macromolecules: Design, synthesis, and characterization. *Macromolecules* 37(2):538–543.
35. Poree DE, Zablocki K, Faig A, Moghe PV, Uhrich KE (2013) Nanoscale amphiphilic macromolecules with variable lipophilicity and stereochemistry modulate inhibition of oxidized low-density lipoprotein uptake. *Biomacromolecules* 14(8):2463–2469.